3D CONVECTION AT INFINITE PRANDTL NUMBER IN CARTESIAN GEOMETRY — A BENCHMARK COMPARISON*

F. H. BUSSE[1], U. CHRISTENSEN[2,3], R. CLEVER[4], L. CSEREPES[5]
C. GABLE[6,13], E. GIANNANDREA[2], L. GUILLOU[7], G. HOUSEMAN[8], H.-C.
NATAF[9], M. OGAWA[10], M. PARMENTIER[11], C. SOTIN[12,14], and B. TRAVIS[13]

[1] *Physikalisches Institut, Universität Bayreuth, Postfach 101251, 95440 Bayreuth, Germany*
[2] *Max-Planck-Institut für Chemie, Postfach 3060, 55020 Mainz, Germany*
[3] *Institut für Geophysik, Universität Göttingen, Herzberger Landstrasse 180, 37075 Göttingen, Germany*
[4] *Institute of Geophysics and Planetary Physics, University of California, Los Angeles, CA 90024, USA*
[5] *Geophysical Department, Eötvös University, Ludovica ter. 2, 1083 Budapest, Hungary*
[6] *Dept. of Earth and Planetary Sciences, Harvard University, Cambridge MA 02138, USA*
[7] *Laboratoire de Dynamique des Systemes Géologiques, IPG, 4 place Jussieu, 75252 Paris Cedex 05, France*
[8] *Dept. of Earth Sciences, Monash University, Clayton VIC 3168, Australia*
[9] *Dépt. TAO, Ecole normale supérieure, 24 rue Lhomond, 75231 Paris 05, France*
[10] *Dept. of Earth Sciences, Ehime University, Ehime 790, Japan*
[11] *Dept. of Geological Sciences, Brown University, Providence, RI 02912, USA*
[12] *Unité CNRS de Géophysique et Géodynamique interne, Université de Paris-Sud, 91405 Orsay Cedex, France*
[13] *Los Alamos National Laboratory, Earth and Environmental Science Div., MS-F665, Los Alamos, NM 87545, USA*
[14] *Laboratoire de Géophysique et Planetologie, Université de Nantes, 2 rue de Houssiniére, 44072 Nantes Cedex 03, France*

We describe the results of a benchmark study of numerical codes designed to treat problems of high Prandtl number convection in three-dimensional Cartesian geometry. In addition, quantitative results from laboratory convection experiments are compared with numerical data. The cases of bimodal convection at constant viscosity and of square cell convection for temperature-dependent viscosity have been selected.

---

* Where two affiliations are given, the second is the present one.
Correspondance and reprint requests to U. Christensen[3]

We compare the Nusselt number, local velocity, temperature, heat flow, topographic and geoid anomalies for stationary solutions. A case of transient time-dependent behavior and the stability limit of bimodal flow are also subject to a comparison. We obtain reasonable agreement among the eight tested codes; and some solutions, which agree within narrow limits, are taken to define a reference for further testing of codes. The results from laboratory experiments agree with the numerical data within the expected range of uncertainty.

1. INTRODUCTION

Thermal convection in the solid mantle of the earth and of terrestrial planets is extensively studied using numerical model calculations. In addition, laboratory experiments with high viscosity fluids are another tool to understand those aspects of thermal convection which are relevant for mantle flow.

In contrast to convective flow in other branches of geophysical fluid dynamics, inertial forces are strictly negligible, but spatial variations of viscosity are of interest. In the past, most of the numerical calculations have been done in two dimensions. However, in recent years the speed of computers has increased sufficiently to make three-dimensional calculations feasible, and many numerical codes have been developed. Because analytical solutions for the convection problem are not available, it is desirable for the verification of codes to establish a "benchmark", i.e., a solution to some standard problem, which is well constrained by a variety of numerical approaches and independent computer programs. In addition, such benchmark comparison can serve to determine advantages that the different numerical codes may have. The present study is part of an ongoing attempt to establish various benchmarks for high Prandtl number convection problems. Blankenbach *et al.* (1989) calculated results for several stationary and time-dependent cases in two-dimensional Cartesian geometry for constant and for variable viscosity. In a similar attempt, Travis *et al.* (1990a) concentrated on comparing in more detail the differences in resolution between the various employed methods. In this paper, we describe the results of a benchmark study for three-dimensional thermal convection in Cartesian geometry.

For a case study of bimodal flow with constant viscosity we get a good coverage with eight different codes. They comprise pure finite difference (FD) techniques, a spectral Galerkin method, and in the majority hybrid spectral and FD techniques. For a case of square cell convection with variable viscosity, three solutions obtained by different techniques provide sufficient coverage to define a benchmark standard.

Three laboratories contributed experimental data on the benchmark cases. The goal was not to try and compete with the 4 digits accuracy to be reported for some quantities in the next section. But the benchmark provided an opportunity to test the ability of various experimental methods to resolve quantitatively the three-dimensional structure. In addition, it was felt interesting to see how different quantities of the numerical solutions were affected by the unavoidable imperfections of the "real world".

2. DEFINITION OF THE BENCHMARK CASES

2.1 General

Consider thermal convection at infinite Prandtl number using the Boussinesq approximation. All material properties are constant, except the viscosity in case 2. Non-dimensional quantities are used according to the scaling in Table 1. The temperature is fixed to $T = 0$ on the upper boundary and $T = 1$ on the lower boundary, and both boundaries are rigid. All side boundaries are planes of mirror symmetry.

2.2 Requested data

All participants have been asked to supply the following results:

(i) The Nusselt number Nu (defined in the usual way as total over conductive heat flow) and the rms-velocity V_{rms} for the entire volume;

(ii) values of the vertical velocity w and the temperature T at specified points at half-depth of the convecting layer;

(iii) the heat flux (temperature gradient) $Q = -\partial T/\partial z$ at specific points at the surface, surface topography Z and geoid anomaly N (including contributions from the deflection of upper and lower boundary but without effects from self-gravitation), where topography and geoid are given in dimensional values, using the dimensional parameters listed in Table 1, with no overlying medium (i.e. no ocean water) assumed, and the mean elevation set to zero;

Table 1   Notation and Scaling

Symbol	Quantity	Scaling factor	Dimens. value SI-units
x, y, z	Cartesian coordinates	h	
a, b	length, width of cell	h	
h	height of cell		$h = 2\,700\,000$
	$(0 < x < a, 0 < y < b, 0 < z < 1,$ z positive upwards)		
t	time	h^2/κ	
$v = (u, v, w)$	velocity	κ/h	
T	temperature	ΔT	
ΔT	temperature contrast		$\Delta T = 3700$
η	viscosity	η_0	
η_0	reference viscosity		8.0198×10^{23} (case 1)
			1.20165×10^{24} (case 2)
r	viscosity contrast (case 2 only)		$r = 20$
k	thermal conductivity		$k = 3.564$
κ	thermal diffusivity		$\kappa = 1.0 \times 10^{-6}$
c_p	specific heat		$c_p = 1080$
α	thermal expansion coeff.		$\alpha = 1 \times 10^{-5}$
ρ	density		$\rho = 3300$
g	gravity constant		$g = 10$
Ra	Rayleigh number	$Ra = \alpha g \rho \Delta T h^3/(\kappa \eta_0)$	

(iv) the following integral, which is related to the deflection of a laserbeam passing in
y-direction through a laboratory tank, for specific values of x and z;

$$\tau(x,z) = \int \partial T/\partial z \, dy,$$

(v) the mean temperature T_m in a horizontal plane at given depth z;
(vi) in case 2 vertical vorticity Ω at specific points.

2.3   Case 1

Case 1a: We consider stationary bimodal convection with constant viscosity. The size
of the cell is $a = 1.0079$, $b = 0.6283$ with height normalized to one (this geometry had
been studied by Frick *et al.* (1983)). The Rayleigh number is 30,000. A stationary
solution with a single upwelling located at $(x, y) = (0, 0)$ and a single downwelling at
(a, b) is calculated. An appropriate initial condition for the temperature could have a
perturbation of the conductive state of the kind

$$\delta T = A[\cos(\pi x/a) + \cos(\pi y/b)]\sin(\pi z).$$

The data (ii)–(v) were requested for the following coordinates:
   (ii) and (iii) $(x, y) = (0, 0), (a, 0), (0, b), (a, b)$.
                 (iv) $(x, z) = (0, 0.25), (a/2, 0.25), (a, 0.25)$
                       (v) $z = 0.75$.

Case 1b: The transition from roll-like convection to bimodal flow is studied as a
function of time. First a single stationary roll with the upwelling flow at $x = 0$ and the
downwelling at $x = a = 1.0079$ is established. This can be done, for example, by
calculating it for a value of b where no bimodal solution exists, like $b = 0.1$, and then the
solution is mapped onto the full cell with the specified b-value of 0.6283. Next a
perturbation of the temperature of the form

$$\delta T = 0.01 \cos(\pi y/b) \sin(\pi z)$$

is added, and the system evolves towards bimodal flow. The difference in temperature
$\Delta T = T(0, 0, 0.5) - T(0, b, 0.5)$ at the non-dimensional times $t = 0.4$ and 1.0 is reques-
ted, scaled by ΔT_∞, which is the value for the stationary bimodal flow.

Case 1c: For $a = 1.0079$ the maximum value of $b = b_{\text{crit}}$, for which rolls are unstable
to bimodal flow, is to be determined. This can be done, for example, by calculating a roll
solution first for different values of b, adding a small perturbation in the y-direction,
and recording its growth or decay.

2.4   Case 2

We study stationary square cell-convection with $a = b = 1.0$ for temperature-depend-
ent viscosity. For the viscosity η we adopt the following law

$$\eta(T) = \exp[Q/(T + G) - Q/(0.5 + G)]$$

where for a given ratio of maximum to minimum viscosity $r = \eta(T=0)/\eta(T=1)$, Q and G are obtained as:

$$Q = [225/\ln(r)] - 0.25\ln(r), \qquad G = [15/\ln(r)] - 0.5.$$

This formula is a good representation for the temperature dependence of laboratory fluids such as corn syrup, which have been employed in the experimental part of this study. The reference viscosity (i.e., the non-dimensional value $\eta = 1$) is for the mean of top and bottom temperatures and the Rayleigh number is defined to this value.

We calculate the stationary solution for a Rayleigh number of 20,000 and a viscosity contrast of $r = 20$. A single rising plume is located at $(x, y) = (0, 0)$. For the data (ii)–(iv) the same coordinates as listed for case 1 are taken. For (v) we take $z = 0.5$ and $z = 0.75$, and for (vi) take the point $(x, y, z) = (0.75, 0.25, 0.75)$.

The original definition of the benchmark comprised a case 2b, in which the stability of square cells depending on the viscosity ratio r was to be studied. However, only a single contribution dealt with this case, which is therefore omitted.

3. DESCRIPTION OF NUMERICAL CODES

A short description of each numerical code is given here. More details can be found in the references. The codes CB, Ch, and Og can treat lateral viscosity differences, while the others do not.

CB — supplied by Clever and Busse is a purely spectral method, employing the scalar potentials for describing the flow. The dependent variables are expanded in all three directions in harmonic functions, where N_T is the total number of modes employed, and the solution to the stationary equations is determined by a Galerkin method. Newton-Raphson iteration is used to solve the resulting non-linear equations (Frick *et al.*, 1983; Busse and Frick, 1985).

Ch — supplied by Christensen is a hybrid spectral and finite difference (FD) method (differences in the vertical direction) employing the scalar potentials for the flow field. For the temperature equation a pure centered FD scheme using the ADI method is employed. To obtain stationary solutions pseudo time-stepping with a step size of 10–30 times the Courant step is used. Solutions for temperature-dependent viscosity are obtained by iteratively determining the coupling of modes of the velocity potentials (Christensen and Harder, 1991).

Cs — supplied by Cserepes is similar to Ch for the case of constant viscosity. The main difference is that the mesh points for temperature and the poloidal potential are not identical, but offset in the vertical direction by 1/2 mesh interval (Cserepes *et al.*, 1988).

Ga — supplied by Gable is a hybrid spectral and FD method applied to the primitive set of flow variables. The temperature solver is the same as in Tr (Gable, 1989; Gable *et al.*, 1991).

Ho — supplied by Houseman is a hybrid spectral and FD method which solves two coupled second-order equations in the vertical (using vector potential components and

vorticity as intermediate variable). An explicit time- and space-centered FD method is used for the temperature equation (Houseman, 1987; Houseman, 1990 a, b).

Og—supplied by Ogawa is a pure FD method employing a non-uniform grid and using primitive variables for the flow field. Momentum and continuity equation are solved by an iterative scheme called SIMPLER algorithm (Patankar, 1980). Implicit central differences are used for the energy equation for the results reported here (Ogawa *et al.*, 1991).

PS—supplied by Parmentier and Sotin solves two coupled Poisson equations (for the poloidal potential with vorticity as intermediate variable) in a pure FD scheme using a multigrid iterative method. Explicit time stepping with a weighted upwind discreti zation for the advective terms is used for the energy equation (Sotin *et al.*, 1993; Parmentier *et al.*, 1993).

Tr—supplied by Travis employs scalar potentials for the flow in a hybrid spectral-FD representation. The temperature equation is solved by an explicit FD scheme which includes a tensor diffusion term to cancel numerical diffusion (Travis *et al.*, 1990b).

4. NUMERICAL RESULTS

4.1   Case 1a

The planform of bimodal steady convection is illustrated in Figure 1. It can be considered as a set of primary convection rolls with their axis perpendicular to the x-direction, which are perturbed by weaker cross-rolls in the y-direction. Ga and Tr
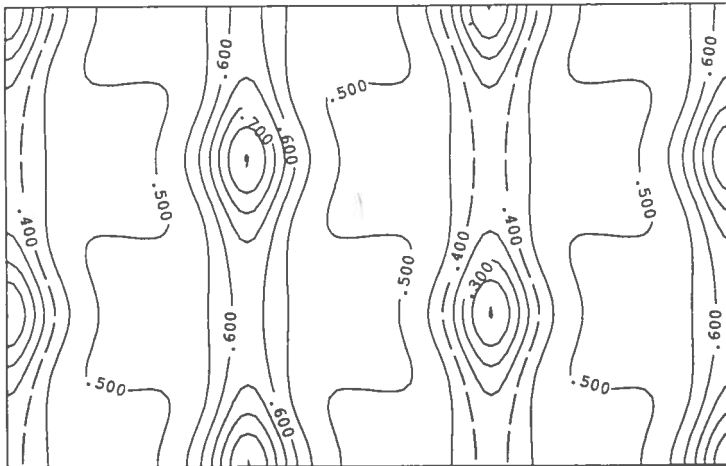

Figure 1   Case 1a: Isotherms at a horizontal plane at $z = 0.5$ taken from a numerical solution by Og. While the calculation has been performed on a block of size $a \times b \times 1$, the symmetry of the solution is used to expand it here to region of $3a \times 3b$.

reported that other planforms are possible depending on the initial condition, like bimodal flow with the stronger roll axis oriented perpendicular to the y-direction, and a kind of distorted hexagonal pattern. Although the pattern shown in Figure 1 is not unique for convection in a box of size $a \times b \times 1$ with mirror symmetry at the side walls, we prefer to study this solution, because numerical work (Frick *et al.*, 1983) and the laboratory results reported later suggest that it is the only stable planform in a layer whose horizontal extent is large compared to its depth.

All participants reported results for case 1a; and most of them did so for more than one grid size. When at least two results for numerical meshes which differed in all three directions by the same factor were provided, an extrapolation of the data was done, assuming a leading error term of second order. Where a sequence of data for successively refined meshes was available (Cs, Ch), a Romberg extrapolation was carried out. Table 2 summarizes the convergence behaviour for some selected quantities, and in Table 3 the "best" results for all requested data are shown, either the value reported for the highest employed resolution, or the extrapolated value. The agreement of the

Table 2 Convergence behavior for selected quantities — case 1a

	Resolution	Nu	$w(0,b,0.5)$	$Q(0,b)$	$Z(0,b)$	$N(0,b)$	$\tau(0,0.25)$
CB	$N_T = 8$	3.6529					
CB	$N_T = 12$	3.5641					
CB	$N_T = 16$	3.5477					
CB	$N_T = 22$	3.54171	40.5003	3.17118			
Ch	$16 \times 16 \times 32$	3.5617	48.418	3.4916	3039.9	187.47	-0.3439
Ch	$24 \times 24 \times 48$	3.5496	43.671	3.2938	2633.6	173.82	-0.3565
Ch	$32 \times 32 \times 64$	3.5445	42.225	3.2378	2511.6	169.62	-0.3603
Ch	$48 \times 48 \times 96$	3.5407	41.249	3.2013	2430.0	166.79	-0.3628
Ch	Extrapol.	3.53741	40.4992	3.17399	2367.8	164.60	-0.36473
Cs	$16 \times 16 \times 24$	3.6112	37.300	3.0927	2109.7	156.07	-0.3623
Cs	$24 \times 24 \times 36$	3.5702	39.118	3.1382	2255.9	160.89	-0.3636
Cs	$32 \times 32 \times 48$	3.5558	39.729	3.1539	2305.3	162.50	-0.3641
Cs	$40 \times 40 \times 60$	3.5492	40.007	3.1611	2327.8	163.23	-0.3643
Cs	Extrapol.	3.53740	40.4986	3.1739	2367.4	164.51	-0.36476
Ho	$32 \times 16 \times 32$	3.541	42.172	3.3217	2650.4	174.10	-0.3663
Ho	$64 \times 32 \times 64$	3.538	40.940	3.2111	2444.5	167.46	-0.3649
Ho	Extrapol.	3.537	40.529	3.1742	2375.9	165.25	-0.3644
Ho	$32 \times 32 \times 32$	3.559	39.954	3.2035	2409.1	165.92	-0.3689
Ga	$16 \times 16 \times 16$	3.4012	47.745	3.5977			
Ga	$24 \times 24 \times 48$	3.5160	41.636	3.2715			
Ga	$32 \times 32 \times 64$	3.5245	41.206	3.2320			
Ga	Extrapol.	3.5355	40.653	3.1812			
Og	$36 \times 22 \times 36$	3.5488	39.53	3.151	2282		-0.3675
PS	$32 \times 16 \times 32$	3.6242	37.404	3.0319			-0.3820
PS	$64 \times 32 \times 64$	3.5575	38.379	3.1017			-0.3775
PS	Extrapol.	3.53528	38.704	3.12496			-0.3760
Tr	$24 \times 24 \times 48$	3.580	38.57	3.0890			-0.3677
Tr	$32 \times 32 \times 64$	3.5636	38.937	3.1070			-0.3670
Tr	Extrapol.	3.543	39.41	3.1301			-0.3662

extrapolated values by Ch and Cs is remarkable. Although the two codes are similar, Cs calculates the temperature on grid points which are offset from the points for the velocity potential, whereas the points are the same in Ch. As a consequence Ch underestimates the strength of the cross-roll with low resolution, and Cs overestimates it, and for most data the results converge from different sides. The extrapolated values from Cs and Ch are corroborated by the extrapolated data supplied by Ho, and the results by CB. In the latter case the convergence behaviour is not known, which prevents an extrapolation of their data. Also for the other contributions the overall agreement is good, indicating that all participating codes perform satisfactorily and are free of serious error. The "best" results for most requested quantities fall within a range of typically 1%, whereas data which are sensitive to the strength of the cross-roll perturbation, such as $w(0, b, 0.5)$, show a larger scatter on the order of $\pm 4\%$. The mid-plane temperatures and velocities should exhibit symmetry, such that for example $w(a, 0, 0.5) = -w(0, b, 0.5)$ and $T(a, 0, 0.5) = 1 - T(0, b, 0.5)$. Redundant values are therefore not reported in Table 2. Most participants found that the symmetry condition was satisfied within 0.1% or better. Ga reports differences between $w(a, 0, 0.5)$ and $-w(0, b, 0.5)$ of about 1–2%, however, they decrease as the square of the mesh interval. Therefore the asymmetry behaves as other truncation errors and is not a serious defect of the method.

The benchmark problem necessarily requires anisotropic mesh spacing ($\Delta x \neq \Delta y \neq \Delta z$). Limited experimentation with different mesh ration (Ho, Table 2) suggests that slightly better results are obtained if the mesh ratios are as near to unity as possible. In particular, Ho-$32 \times 32 \times 32$ ($\Delta x/\Delta z = 1.0079$ and $\Delta y/\Delta z = 0.6283$) generally gave poorer results than Ho-$32 \times 16 \times 32$ with $\Delta y/\Delta z = 1.2566$, even though the resolution is nominally better.

In Table 3 we also try to give an estimate for the exact solution. The data supplied by CB, Ch, Cs, and Ho have been used to derive it. This does not imply that we consider the respective codes as superior compared to others. They have been selected because these contributors supplied a sequence of results with increasing resolution, showing a well-documented convergence behaviour, which allows (except for CB) the extrapolation to the asymptotic value. The best estimate has been picked from the two closest results, oftern Ch and Cs. The generally close agreement of the results from further independently conceived codes is a safeguard against minor systematic errors. The uncertainty quoted in Table 3 covers the range of the three extrapolated solutions Ch, Cs, Ho, and (except for the Nusselt number) the best result by CB.

4.2 Case 1b

The typical evolution of the temperature difference at the mid-plane due to the growth of the cross roll is characterized by an initial oscillatory behaviour (Figure 2). The reason for this is most probably that the imposed depth-dependence of the perturbation does not agree with the characteristic depth-dependence of the cross-roll (or its eigen-function for infinitesimal amplitude). The oscillations die out within 0.1 thermal diffusion times, with a smooth growth of the cross-roll, which is completed within 95% after one thermal diffusion time.

Table 3 Best results for all quantities-case 1a

| Resolution	CB $N_T = 22$	Ch Extrapol	Cs Extrapol	Ga Extrapol	Ho Extrapol	Og $36 \times 22 \times 36$	PS Extrapol	Extrapol	Trbest estimate
Nu	3.54171	3.543741	3.53740	3.5355	3.537	3.5488	3.5353	3.543	3.5374 ± 0.0005
vrms	40.9991	40.9992	40.9986		40.995	41.037	40.8456		40.999 ± 0.004
w(0,0.5)	116.625	116.626	116.629	116.505	116.596	117.16	116.645	117.34	116.625 ± 0.030
w(0,b,0.5)	40.500	40.499	40.495	40.653	40.529	39.53	38.704	39.41	40.500 ± 0.030
T(0,0,0.5)	0.80129	0.80130	0.80130	0.80095	0.80131	0.8016		0.80280	0.80130 ± 0.00005
T(0,b,0.5)	0.61876	0.61877	0.61875	0.61917	0.61881	0.6161		0.61648	0.61876 ± 0.00005
Q(0,0)	6.73478	6.71267	6.7126	6.7074	6.7485	6.806	6.7567	6.7499	6.7127 ± 0.0500
Q(a,0)	1.49799	1.50800	1.5080	1.5071	1.5019	1.517	1.5300	1.5213	1.5080 ± 0.0500
Q(0,b)	3.17118	3.17399	3.1739	3.1812	3.1742	3.151	3.1250	3.1301	3.1740 ± 0.0500
Q(a,b)	0.70988	0.71407	0.7140	0.7153	0.70893	0.700	0.7146	0.7098	0.7140 ± 0.0500
Z(0,0)		8180.3	8181.3		8189.5	8302			8180 ± 12
Z(a,0)		−5572.7	−5571.9		−5583.6	−5559			-5572 ± 12
Z(0,b)		2367.8	2367.4		2375.9	2282			2369 ± 12
Z(a,b)		−9107.4	−9107.1		−9119.6	−9208			-9107 ± 12
N(0,0)		345.50	345.34		346.50				345.5 ± 1.5
N(a,0)		−0240.90	−0240.77		−0241.77				-0240.9 ± 1.5
N(0,b)		164.60	164.51		164.25				164.6 ± 1.5
N(a,b)		−0373.89	−0373.73		−0375.01				-0373.9 ± 1.5
τ(0,0.25)	−0.36493	−0.36473	−0.36476		−0.3644	−0.3675	−0.3760	−0.3662	-0.3648 ± 0.0005
τ(a/2,0.25)	−0.12995	−0.12969	−0.12967		−0.1300	−0.1295		−0.1278	-0.1297 ± 0.0005
τ(a,0.25)	−0.11120	−0.11038	−0.11036		−0.1101	−0.1066		−0.1120	-0.1104 ± 0.0005
T_m(0.75)	0.52149	0.52147	0.52148	0.52269	0.52151	0.5214	0.52090	0.52090	0.52148 ± 0.00003

F. H. BUSSE *et al.*
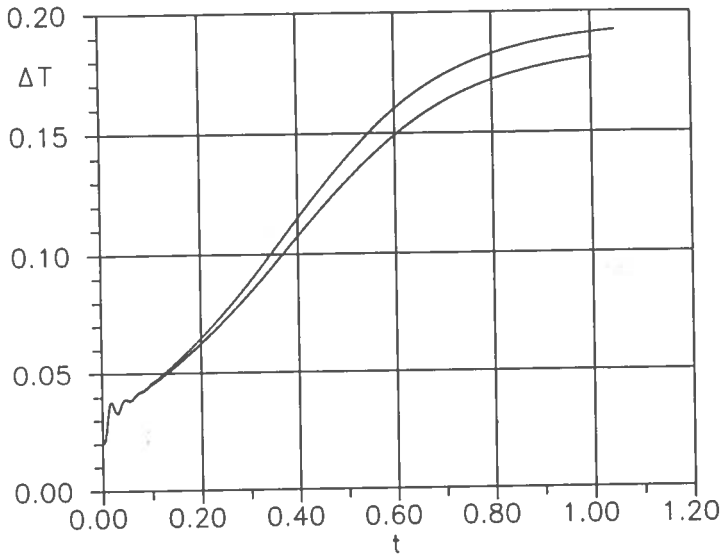
Figure 2 Case 1b: Evolution of the temperature difference $\Delta T = T(0,0,0.5) - T(0,b,0.5)$ as a function of time. Results by Cs with $16 \times 16 \times 24$ grid points for the upper line and $32 \times 32 \times 48$ for the lower line.

The quantitative comparison (Table 4) reveals a quite large scatter. A systematic study by Ch showed that the result is mainly sensitive to the spatial resolution, and much less to the choice of the time-step (in terms of fractions of the Courant time step), even for a method which is only first order correct in time. Because the results by Ch and Cs converge from different sides and the extrapolated values agree well, they have been taken to derive a best estimate. However, because of the deviation of the other

Table 4 Results for case 1b

	Resolution	$\Delta T(t=0.4)/\Delta T(\infty)$	$\Delta T(t=1.0)/\Delta T(\infty)$
CB	$N_T = 14$	0.5470	0.9674
Ch	$16 \times 16 \times 32$	0.4389	0.8574
Ch	$24 \times 24 \times 48$	0.5096	0.9398
Ch	$32 \times 32 \times 64$	0.5381	0.9562
Ch	$48 \times 48 \times 96$	0.5595	0.9652
Ch	Extrapol.	0.5772	0.9708
Cs	$16 \times 16 \times 24$	0.5879	0.9765
Cs	$32 \times 32 \times 48$	0.5782	0.9721
Cs	Extrapol.	0.5750	0.9706
Ho	$32 \times 32 \times 32$	0.5495	0.9630
PS	$32 \times 32 \times 32$	0.6790	0.9917
Tr	$24 \times 24 \times 48$	0.6058	0.9883
Best estimate		0.576 ± 0.03	0.9706 ± 0.010

data, we must allow for larger error limits than in Case 1a. The cause for the large deviations is not clear.

4.3   Case 1c

When determining the instability of rolls against a cross-roll perturbation in the way suggested in Section 2, at first transient oscillations are found as described in the previous section. After they have died out within about 0.15 diffusion times, a clear exponential growth or decay of the perturbation was found. The agreement for the critical value b for the instability of the rolls between the five contributing codes is good (Table 5) and allows to determine a best estimate within a reasonably narrow uncertainty range.

4.4   Case 2

The planform for the case of temperature dependent viscosity is shown in Figure 3. It consists of isolated hot rising plumes imbedded in a square of sheet-like descending flow with concentrations at the junctions between sheets. According to the laboratory experiments by White (1988), the square pattern would be stable in a layer of large horizontal dimensions up to a Rayleigh number of 20,000, as considered here, but it would evolve into a spoke pattern at higher Rayleigh number.

As would be expected, fewer contributions deal with this case, but the agreement between the three submitted solutions is remarkably good. The data from CB and Ch show clear convergence, which allows for Ch again an extrapolation to values, which are in good agreement with the trend visible in the CB data, for which a formal extrapolation is not possible (Table 6). The resolution for the two data sets supplied by Og is not sufficiently distinct to allow an extrapolation, however, the agreement with the other results is satisfactory. The agreement is also good for such aspects of the solution, which are peculiar to the temperature dependence of viscosity, as local values of the vertical vorticity (Table 7). Because the three numerical approaches are completely different, we think that we can define the benchmark solution also for this case

Table 5   Results for case 1c

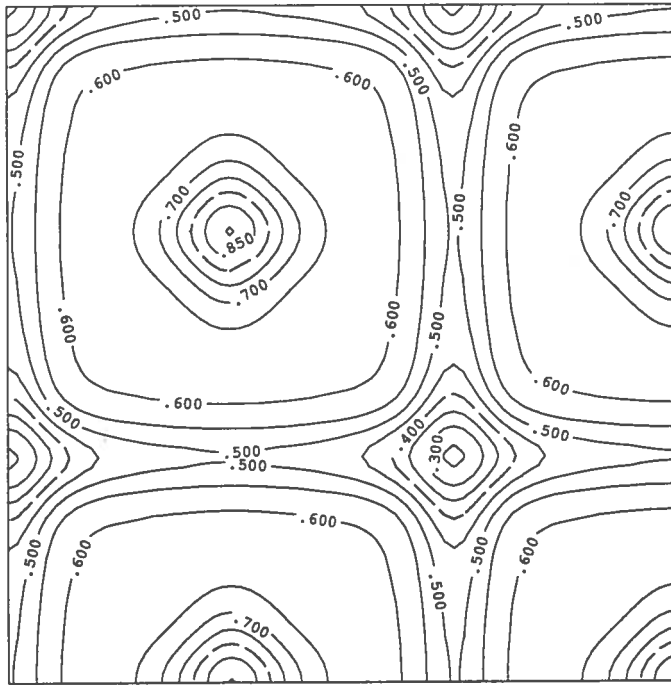|	Resolution	b_{crit}
CB	$N_T = 14$	0.813
Ch	$16 \times 16 \times 24$	0.7538
Ch	$24 \times 24 \times 48$	0.7858
Ch	$32 \times 32 \times 64$	0.7917
Ch	$48 \times 48 \times 96$	0.8053
Ch	Extrapol.	0.8120
Cs	$16 \times 16 \times 24$	0.8045
Cs	$32 \times 32 \times 48$	0.8074
Cs	Extrapol.	0.8084
Ho	$32 \times 32 \times 32$	0.8155
Tr	$32 \times 26 \times 32$	0.8131
Best estimate		0.812 ± 0.04

F. H. BUSSE *et al.*

Figure 3 Case 2: Isotherms at the horizontal plane at $z = 0.5$ taken from a numerical solution by Og. The domain size is $3a \times 3a$.

with great confidence. The extrapolated values from Ch are taken as the best estimate for the exact solution (Table 7). The difference to the results by Og, and, where available, by CB, have been used to set the uncertainty limits, except where the close agreement of Ch and Og appeared to be accidental:

Table 6 Convergence behavior for selected quantities — case 2

	Resolution	Nu	$w(0,0,0.5)$	$Q(0,0)$	$Z(0,0)$	$N(0,0)$
CB	$N_T = 12$	3.0553	150.9			
CB	$N_T = 18$	3.0464	163.6			
CB	$N_T = 26$	3.0420	165.6			
Ch	$16 \times 16 \times 32$	3.0729	162.41	5.8969	11384	554.0
Ch	$24 \times 24 \times 48$	3.0547	163.99	5.8652	11111	542.3
Ch	$32 \times 32 \times 64$	3.0480	164.72	5.8522	11009	538.1
Ch	$48 \times 48 \times 64$	3.0432	165.34	5.8423	10932	535.0
Ch	Extrapol.	3.03927	165.91	5.8339	10869	532.49
Og	$30 \times 30 \times 30$	3.0466	166.02	5.910	10898	
Og	$36 \times 36 \times 36$	3.0441	166.95	5.903	10890	535.6

Table 7 Best results for all quantities-case 2

	CB	Ch	Og	Best estimate
Resolution	N_T	Extrapol	$36 \times 36 \times 36$	
Nu	3.0420	3.03927	3.0441	3.0393 ± 0.0050
vrms		35.132	35.165	35.13 ± 0.05
$w(0, 0, 0.5)$	165.6	165.91	166.95	165.9 ± 1.0
$w(0, b, 0.5)$		-26.72	-26.72	-26.72 ± 01
$w(a, b, 0.5)$		-58.23	-58.25	-58.23 ± 0.1
$T(0, 0, 0.5)$		0.90529	0.9059	0.90529 ± 0.0010
$T(0, b, 0.5)$		0.49565	0.4951	0.49565 ± 0.0010
$T(a, b, 0.5)$		0.23925	0.2386	0.23925 ± 0.0010
$Q(0, 0)$		5.8339	5.903	5.834 ± 0.015
$Q(a, b)$		1.7136	1.702	1.714 ± 0.015
$Q(a, b)$		0.7684	0.754	0.768 ± 0.015
$Z(0, 0)$		10869	10890	10870 ± 150
$Z(a, b)$		-4145	-4203	-4145 ± 150
$Z(a, b)$		-12811	-12933	-12810 ± 150
$N(0, 0)$		532.5	535.6	532.5 ± 10.0
$N(0, b)$		-137.6	-140.4	137.6 ± 10.0
$N(a, b)$		-626.2	-635.3	-626.2 ± 10.0
$\tau(0, 0.25)$		-0.5059	-0.5060	-0.5059 ± 0.0040
$\tau(a/2, 0.25)$		-0.1921	-0.1955	-0.1921 ± 0.0040
$\tau(a, 0.25)$		-0.1388	-0.1376	-0.1388 ± 0.0040
$T_m(0.75)$		0.56593	0.5660	0.56593 ± 0.00100
$T_m(0.50)$		0.58158	0.5807	0.58158 ± 0.00100
$\Omega(0.75, 0.25, 0.75)$		-11.125	-11.36	-11.125 ± 0.25

5. COMPARISON OF LABORATORY DATA AND NUMERICAL RESULTS

5.1 Experimental set-ups

In all three contributing labs, the working fluid is enclosed in a transparent rectangular frame sandwiched between thick horizontal metal plates. The temperature in these plates is measured with imbedded thermocouples. A transparent working fluid is used: silicon oil for the isoviscous case (case 1a), and sugar syrup for the case with temperature-dependent viscosity (case 2a).

Simple visualisation techniques are used to give a rough idea of the convection pattern: the shadowgraph method gives access to temperature variations, though integrated along the x or y direction, while the velocity structure is obtained using passive tracers (aluminum flakes or hollow glass spheres). The number of convection cells in the x and y directions can usually be deduced from these crude observations.

In all cases, the system was left free to choose the aspect ratio which developed from an initial temperature condition which could not be accurately regulated. Therefore, the dominant aspect ratio was usually different from the one specified in the benchmark definition.

5.2   Quantitative techniques

In the lab, there is no problem obtaining a three-dimensional convective structure. The problem rather rests in its identification and measurement. Very few techniques yield local values everywhere in the fluid. Nevertheless, more global quantities, such as the Nusselt number, or the vertical profile of horizontally-averaged temperature, are often as important for applications to geophysical problems.

In this report, results from several different techniques are presented. Local velocities $w(x, y, z)$ are measured from stroboscoped streak photographs of passive tracers. Vertical profiles of horizontally-averaged temperature $T_m(z)$ are obtained by measuring the electrical resistance of a platinum wire. Integrated (over y) temperature gradients $\tau(x, z)$ are deduced from the deflection of a laser beam. The Nusselt number is derived from the $T_m(z)$ profile, or measured directly from the total heat power fed into the tank. The techniques will be discussed further and evaluated with the presentation of the different results.

5.3   Case 1a (Isoviscous bimodal convection)

This case was treated in only one lab (Nataf). The experimental parameters are listed in Table 8. The fluid is silicon oil. The set-up and procedure are similar to those described in Nataf *et al.* (1988).

The measurements were taken between 2.5 and 5 days (30 and 60 diffusion times) after convection started. The pattern was seen to be bimodal with 7 rolls in the x direction, and 5 in the y direction. But the width of the rolls could differ by as much as a factor of 2, with smaller rolls on the side-walls. This situation appeared to persist during the entire run.

5.3.1   Velocity measurements

Local velocity measurements were taken, using a very simple method: the fluid contains tiny aluminium flakes; a $y = $ const. slice of fluid is illuminated; a long-exposure photograph is taken. The length of the streak on the picture is proportional to the projection of the velocity vector in the illuminated xz-slice. The light is stroboscoped, so that by counting the number of dots in the track, one can check that the flake remained in view during the complete exposure. Figure 4 gives an example of a slice near $y = b$, with x between $-a$ and a. The velocity in the central uprising current ($x = 0$) is clearly much

Table 8   Experimental parameters

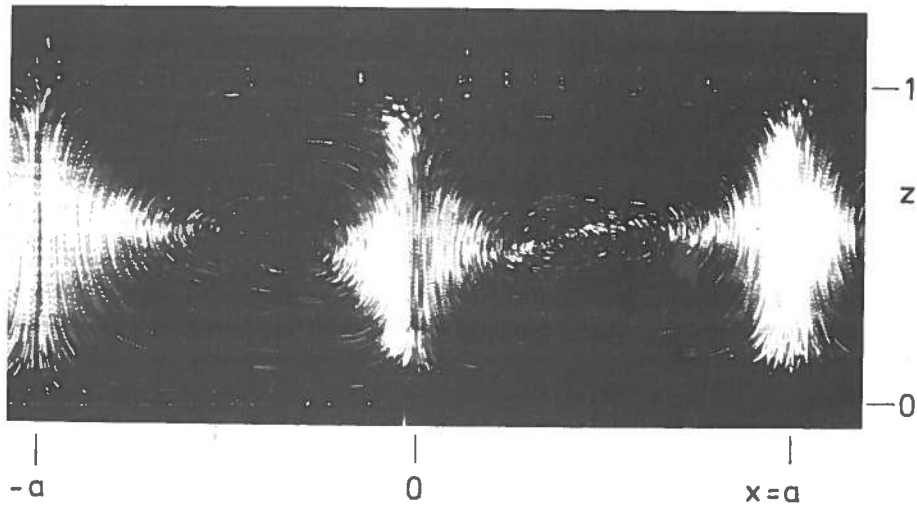| Laboratory	depth (cm)	aspect ratio	fluid	viscosity at mean $T(P\ a.s)$	Ra	ΔT (K)	r_η
Case 1a							
Nataf	2.9	8.6×4.3	silicon oil	0.93	30,000	14.4	(1.33)
Case 2a							
Giannandrea	6.5	7.3×7.3	sugar syrup	18.11	16,880	22.4	18.5
Guillou	4.07	8×8	sugar syrup	3.82	20,400	27.9	19.6

Figure 4 Case 1a: streak photograph of an xy-slice of fluid near $y = b$. There is an uprising current in the center $(x = 0)$, and downwellings on both sides $(x = \pm a)$. The picture was obtained by taking a 16 second-exposure of the tank, while the xz-slice was illuminated by light pulses of 1 sec duration interrupted by dark intervals of 1 sec. Aluminum flakes entrained in the fluid leave tracks, consisting of 8 bright dots. The length of a track is proportional to the component of the local velocity in the xz plane.

smaller than in the downwelling currents on the sides $(x = \pm a)$. This a consequence of the three-dimension pattern: the slice is close to a downwelling sheet of the cross-rolls.

A tedious analysis of a series of pictures for different y values yield the following information: the flow is bimodal, with $a = 1.17$, and $b = 0.63$. The axes of both sets of rolls appear, locally, to deviate by about 10° from being parallel to the walls of the tank, and there are indications of some asymmetry. The vertical velocities $w(0, 0, 0.5) = 106$, $w(a, 0, 0.5) = 45$, and $w(0, b, 0.5) = -45$, and $w(a, b, 0.5) = -112$ were derived from the streak photographs. They agree within 12% with the numerical values of Table 3, which can be considered as good given the experimental uncertainties. They indicate, however, that the cross-rolls are less developed in the lab than in the numerical experiments.

5.3.2 *Vertical profile of horizontally-averaged temperature*

The horizontally-averaged temperature at a given depth can be obtained from the average electrical resistance of a platinum wire suspended at a given depth and cutting the convection pattern at an oblique angle (e.g., Richter *et al.*, 1983). By moving the wire to different depths (with about 5 sec. time delay) one gets a vertical profile. The method requires some calibration. Here, this was done by measuring a reverse (conductive) profile, and an isothermal one. Figure 5 shows two profiles obtained for case 1a: one when moving the wire up, the other one when moving it down. Details of the numerical profile are nicely reproduced, but there appears to be a systematic difference between the up- and down-profiles, as well as a global shift to lower temperatures. The latter is
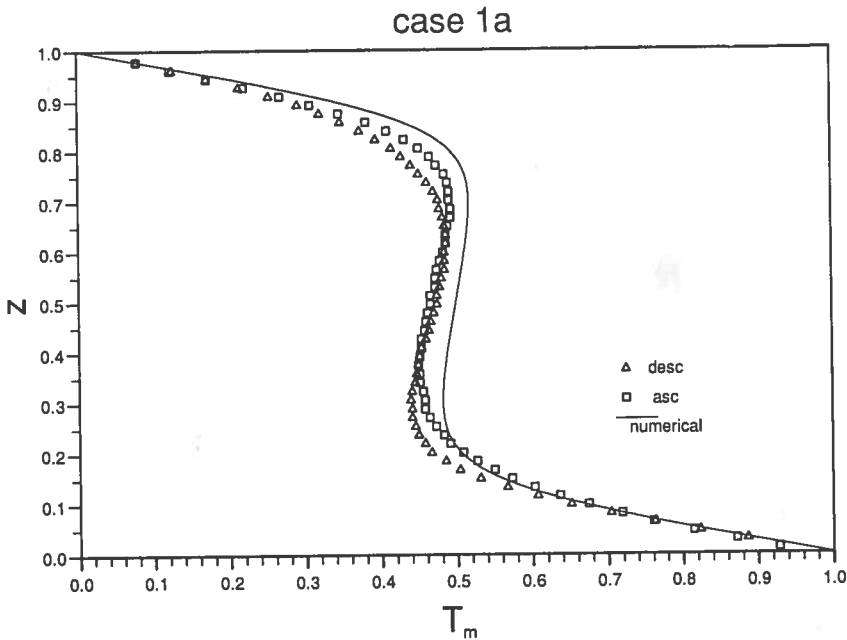
F. H. BUSSE *et al.*

case 1a

Figure 5 Case 1a: vertical profile of the horizontally-averaged temperature. The asc (desc) profile is obtained by moving up (down) a platinum wire, which runs in a horizontal plane in the fluid. The wire rests for 5 seconds after each move, before the measurement is taken. The electrical resistance of the wire is proportional to temperature. Note the systematic difference between the two profiles.

probably due to a calibration error. The former effect is more serious: it indicates that the flow is perturbed by the presence of the wire, as one could expect indeed in a very viscous fluid. Note that this effect is even more pronounced in experiments with a nearly stress-free surface (Giannandrea and Christensen, 1993).

The Nusselt number can easily be measured from the slope of the profile at the top or bottom. Both profiles yield a mean value $Nu = 3.5$, compatible with the numerical result. However, there appears to be again a strong bias, since for the descending profile, the top and bottom boundary layers yield very different values (3.0 versus 4.0).

5.3.3 *Profiles of y-integrated temperature gradients*

The deflection of a laser beam, entering the tank horizontally parallel to the y-direction, is proportional to the temperature-gradient vector in the xz-plane, integrated along the y-direction (e.g., Nataf *et al.*, 1981). Some calibration is needed. It is easily obtained by running a reverse (conductive) gradient, and an isothermal one. The x-profiles have been measured at different depths. Although no direct information is available from these data on structure in the y-direction, it is interesting to note that the horizontal gradients should only reflect structure in the x-direction, whereas vertical gradients are, in addition, sensitive to rolls in the y-direction.

Figure 6 compares experimental and numerical profiles of the horizontal and vertical gradients of temperature at two different depths: $z = 0.25$ and $z = 0.5$. The numerical profiles were computed by Ch on a $32 \times 32 \times 64$ grid, using the a and b values derived from the experimental velocity measurements ($a = 1.17$, $b = 0.63$). For comparison, numerical profiles for two-dimensional-rolls with the same a value are also given.

On the $z = 0.25$ profile of horizontal temperature gradient, one recognises the signature of an uprising current at $x = 0$: isotherms are nearly vertical and closely packed, giving rise to high values of the horizontal gradient, changing sign in the center of the uprising. The gradients in the core of the convection cells are much smaller.

Overall, the agreement between the numerical and experimental profiles is very good. Especially interesting is the profile of vertical gradient at $z = 0.25$. The numerical experiments show that the shape of this profile is very sensitive to the existence of cross-rolls. This is well recovered by the experimental profile. However, there is again some indication, from all profiles, that the cross-roll structure is slightly less developed in the lab than in the computations. This is probably a consequence of the stronger confinement in the y-direction imposed by the size of the tank.

5.4 Case 2a (Temperature-dependent viscosity square convection)

This case was treated in two labs (Giannandrea, and Guillou). Both used sugar syrup as a working fluid. The experimental parameters are given in Table 8.

A square pattern was probably obtained by Giannandrea. From the limited streak observations it is not clear if the dimension of the squares was approximately $a = b = 1.5$ or 0.75; at any rate it differed from unity as prescribed in the benchmark definition. Guillou did not obtain any steady-state, even after 8 days (50 diffusion times). At some point a fairly regular pattern, possibly squares, with $a = 0.8$ was observed, but did not stay.

5.4.1 Nusselt number

The apparatus of Giannandrea was especially designed for measuring the Nusselt number. A description can be found in Giannandrea and Christensen (1993) the bottom plate is heated by a thin foil, which consists of a precision resistance alloy. A guard heating system ensures that all the heat entering the foil goes into the tank. Heat flowing into the side-walls is corrected for. The Nusselt number is then deduced from the total ohmic heat of the foil, and the measured temperature of the top and bottom plates. The Nusselt number obtained for case 2a was $Nu = 3.03 \pm 0.05$. This value is the interpolation of several experimental results with neighbouring values of Rayleigh number and viscosity ratio (Giannandrea and Christensen, 1993). The closest actual experiment is summarized in Table 8. It yielded a Nusselt number of 2.93. The interpolated Nusselt number is apparently in very good agreement with the numerical experiments, however, for the likely cell size in the experiment of $a = b = 0.75$ numerical calculations by Ch gave a Nusselt number of 3.18, i.e., a deviation of 5% from the experimental value. Given the uncertainty in physical properties of the fluid, such as its thermal conductivity, an error of this order is plausible.
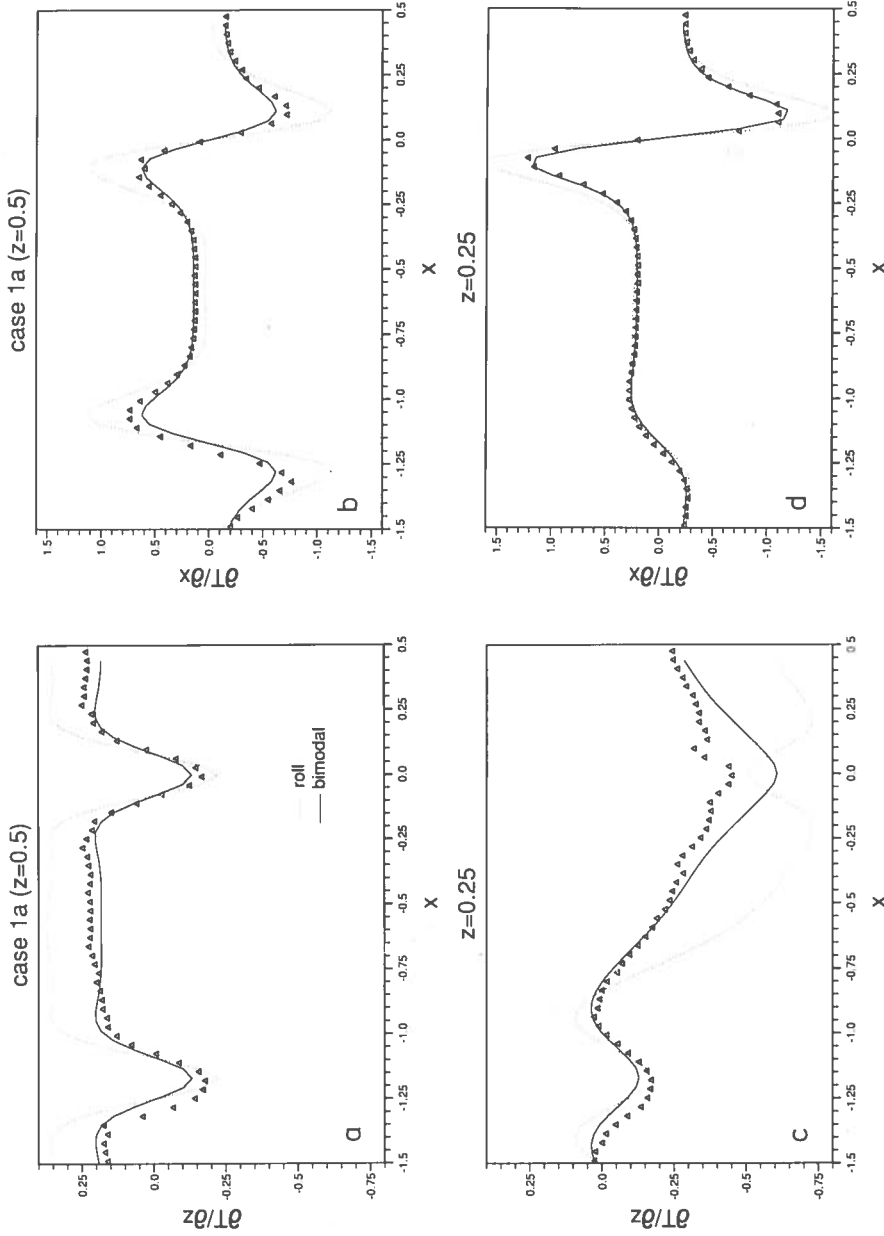
F. H. BUSSE *et al.*

Figure 6 Case 1a: comparison of numerical (solid line, "bimodal") and experimental (open symbols) horizontal profiles of temperature gradients. Also shown are the numerical profiles for a two-dimensional computation with the same value of Rayleigh number (dotted line, "roll"). (a) and (b) $z = 0.5$; (c) and (d) $z = 0.25$. (a) and (c) horizontal gradient of temperature $\int \partial T / \partial x \, dy / \int dy$; (b) and (d) vertical gradient $\int (\partial T / \partial z \, dy / \int dy$.

As mentioned above, the experiment by Guillou did not reach a steady state. In his case, temperatures are measured at fixed positions in the tank by thermocouple probes running in the fluid (see a description in Guillou, 1992). Conceivably the unsteadiness may arise because (1) the temperature probes perturb the flow, or (2) because the tank dimensions cannot accommodate the preferred wavelength of stationary square cell convection. It may also play a role that accoring to White (1988) square cells are close to their stability limit at a Rayleigh number of 20,000. The Nusselt number was deduced from the temperature difference between the upper plate and a row of 6 thermocouples at a depth $z = 1 - 0.075$. The Nusselt number showed large variations with time, with values from 2.6 to 4.6, and these variations appear to correspond to the spatially unstable pattern.

6. CONCLUSIONS

Our comparison study has shown that today reliable technical means for modeling high Prandtl number convection in three dimensions are available. For steady convection, the agreement among the participating codes concerning global properties, such as the Nusselt number, is typically of the order of 1% or better. As would be expected, data which are sensitive to slight differences in the three-dimensional pattern, such as the strength of the cross-rolls in bimodal convection, are subject to larger differences, but these are still at a tolerable level for geophysical applications. Our study also shows the power of extrapolating a sequence of successively higher resolved results to obtain very high precision data. The very good agreement of extrapolated data obtained by various codes makes us very confident of the correctness of the "bench mark solution" which should be useful for the future verification of three-dimensional convection codes Also the case of temperature-dependent viscosity can be reliably resolved, as is demon strated by the good agreement of results from three completely different methods.

A special interest in performing three-dimensional modeling lies in the determination of the planform of convection. The agreement for the critical wavelength of cross-rolls suggests that the issue of pattern selection is probably well taken by all codes contributing to case 1c. However, the difficulty that some participants had to obtain the same bimodal pattern for case 1a shows that a given solution can be non-unique and dependent on the initial conditions.

Compared to the previous two-dimensional benchmark study (Blankenbach et al., 1989), the level of difference between the reported results is some-what larger at a similar level of numerical resolution. One explanation is that in the two-dimensional benchmark most codes were finite element methods which employed higher resolution in the boundary layers, which enhances the accuracy, whereas in the present study the resolution is always uniform. Another explanation is that in a small two-dimensional domain the possible geometry of the flow is strongly constraints. The additional degree of freedom in three-dimensional weakens the constraints on the precise distribution of the flow, which is evident for case 1a in the rather large differences found for the strength of the cross roll.

The comparison of the numerical results with laboratory measurements brings to light several interesting issues.

Most often the physical system appears to be fairly "lazy", in that it can accommodate a somewhat non-symmetrical pattern for a very long period of time. Conversely, small perturbations, such as sidewall effects or those induced by plunging thermocouples may have a strong influence on the system. By analogy with crystallography, the numerical experiment can be seen as the "ideal" brick of the physical system, which contains all kinds of defects in the real world.

Despite these differences in the pattern of convection, the values of those parameters that could be measured in the lab agree quite well with the numerical results.

Several experimental methods could be tested. Streak photographs of passive tracers are a very good tool for determining the pattern of convection (when it cannot be observed more directly from the top of the tank). It also yields a surprisingly good quantitative velocity field. However, for many geophysical applications, the temperature field is often more important. Vertical profiles of the horizontally-averaged temperature were obtained using a platinum wire. The method is very sensitive and nicely picks up details of the numerical profiles. However, there are clear indications that the moveable wire perturbs the flow, thereby producing systematic biases. Considering how useful the method proves to be in many applications, it is important to assess how large these biases are in particular experiments. The deviation of a laser beam is very sensitive to the thermal structure of convection. Although it integrates the information along one direction, it was found that it could be used to discriminate between rolls and bimodal convection. The determination of the Nusselt number based on the measurement of the total heat power input was found to give results within the expected experimental uncertainty. Our comparison study suggests that numerical and laboratory experiments can complement each other in many applications, and that semi-quantitative or better agreement can be achieved.

References

Blankenbach, B. and 13 more authors, "A benchmark comparison of mantle convection codes", *Geophys. J. Int.* **98**, 23–38 (1989).

Busse, F. H. and Frick, H., "Square pattern convection in fluids with strongly temperature-dependent viscosity", *J. Fluid Mech.* **150**, 451–465 (1985).

Christensen, U. and Harder, H., "3-D convection with variable viscosity", *Geophys. J. Int.* **104**, 213–226 (1991).

Cserepes, L., Rabinowicz, M. and Rosenberg-Borot, C., "Three-dimensional infinite Prandtl-number convection in one and two layers and implications for the earth's gravity field, "*J. Geophys. Res.* **93**, 12009–12025 (1988)

Frick, H., Busse, F. H. and Clever, R. M., "Steady three-dimensional convection at high Prandtl number", *J. Fluid Mech.* **127**, 141–153 (1983).

Gable, C. W., "Numerical models of plate tectonic and mantle convection in three dimensions, Harvard University", PhD thesis, Cambridge MA (1989).

Gable, C. W., O'Connell, R. J. and Travis, B. J., "Convection in three dimensions with surface plates: Generation of toroidal flow", *J. Geophys. Res.* **96**, 8391–8405 (1991).

Giannandrea, E. and Christensen, U. "Variable viscosity convection experiments with stress-free upper boundary and implications for the heat transport in the Earth's mantle", *Phys. Earth Planet. Inter.* **78**, 139–152 (1993).

Guillou, L., " Les continents et la convection dans le manteau terrestre", Thèse de Doctorat de l'Université Paris 7, Octobre (1992).

Houseman, G., "TDPOIS, a vector processor routine for the solution of the three-dimensional Poisson and biharmonic equations in a rectangular prism", *Camp. Phys. Comm.* **43**, 257–267, (1987).

Houseman, G. A., "Boundary conditions and efficient solution algorithms for the potential function formulation of the three-dimensional viscous flow equation", *Geophys. J. Int.* **100**, 33–38 (1990a).

Houseman, G. A., "The thermal structure of mantle plumes: axisymmetric or triple junction?," *Geophys. J. Int.* **102**, 15–24 (1990b)

Nataf, H.-C., Moreno, S. and Cardin, Ph., "What is responsible for thermal coupling in layered convection?," *J. Phys. France* **49**, 1707–1714 (1988).

Nataf, H.-C., Froidevaux, C., Levrat, J.-L. and Rabinowicz, M., "Laboratory experiments: effect of lateral cooling and generation of instabilities in the horizontal boundary layers", *J. Geophys. Res.* **86**, 6143–6154 (1981).

Ogawa, M., Schubert, G. and Zebib, A., "Numerical simulation of 3-D thermal convection of a strongly temperature-dependent viscosity fluid," *J. Fluid Mech.* **233**, 299–328 (1991).

Parmentier, E. M., Sotin, C. and Travis, B. J., "Turbulent 3D thermal convection in an infinite Prandtl number, volumetrically heated fluid: Implications for mantle dynamics," *Geophys. J. Int.*, in press (1993).

Patankar, S. V., *Numerical heat transfer and fluid flow*, Hemisphere Publ. Co., New York, 197 pp., (1980).

Richter F. M., Nataf, H.-C. and Daly, S. F., "Heat transfer and horizontally averaged temperature of convection with large viscosity variations," *J. Fluid Mech.* **120**, 173–192 (1983).

Sotin, C., Parmentier, E. M., Carey-Gailhardis, E. and Stocklet, P., "A 3D multigrid Poisson solver on the Connection machine: application to convection within planetary interiors, submitted to *J. Comp. Phys.* (1993).

Travis, B., and 8 more authors, "A benchmark comparison of numerical methods for infinite Prandtl number convection in two-dimensional Cartesian geometry," *Geophys. Astrophys. Fluid Dynam.* **55**, 137–160 (1990a).

Travis, B., Olson, P. and Schubert, G., "The transition from two-dimensional to three-dimensional planforms in infinite-Prandtl number thermal convection," *J. Fluid Mech.* **216**, 71–91 (1990b).

White, D., "The planforms and onset of convection with a temperature dependent viscosity", *J. Fluid Mech.* **191**, 247–286 (1988).